JPE 15-6-3

http://dx.doi.org/10.6113/JPE.2015.15.6.1438
ISSN(Print): 1598-2092 / ISSN(Online): 2093-4718

Analysis and Implementation of a DC-DC Converter for Hybrid Power Supplies Systems

Lung-Sheng Yang† and Chia-Ching Lin*

†,*Department of Electrical Engineering, Far East University, Tainan City, Taiwan

Abstract

A new DC-DC power converter is researched for renewable energy and battery hybrid power supplies systems in this paper. At the charging mode, a renewable energy source provides energy to charge a battery via the proposed converter. The operating principle of the proposed converter is the same as the conventional DC-DC buck converter. At the discharging mode, the battery releases its energy to the DC bus via the proposed converter. The proposed converter is a non-isolated high step-up DC-DC converter. The coupled-inductor technique is used to achieve a high step-up voltage gain by adjusting the turns ratio. Moreover, the leakage-inductor energies of the primary and secondary windings can be recycled. Thus, the conversion efficiency can be improved. Therefore, only one power converter is utilized at the charging or discharging modes. Finally, a prototype circuit is implemented to verify the performance of the proposed converter.

Key words: High step-up converter, Hybrid power supplies system, Renewable energy

I. INTRODUCTION

The use of the fossil fuels causes environmental pollution and ecological problems. In addition, carbon-dioxide emissions result in global warming. Therefore, the development and application of renewable energy sources has become very important [1]-[10]. Renewable energies include wind power, solar power, ocean energy, hydrogen energy, hydro energy and so on. Fig. 1(a) shows the conventional renewable energy and battery hybrid power supply system. It can be seen that the battery is charged from a renewable energy source via two converters [11]-[17]. Therefore, the conventional hybrid power supply system results in energy waste. For this reason, this paper presents a new DC-DC converter for three-port renewable energy and battery hybrid power supplies systems, as shown in Fig. 1(b). It can be seen that the battery is only via one converter at the charging or discharging mode. Fig. 2 shows the circuit configuration of the proposed converter. The pulse-width modulation (PWM) technique is used for the proposed converter. At the charging mode, the renewable energy source provides its energy to charge the battery via the proposed converter. Here the proposed converter is a conventional DC-DC buck converter [18], [19]. At the discharging mode, the battery releases its energy to the DC bus via the proposed converter. Meanwhile, this converter is a non-isolated high step-up DC-DC converter [20]. The coupled-inductor technique is used to achieve a high step-up voltage gain by adjusting the turns ratio. Moreover, the

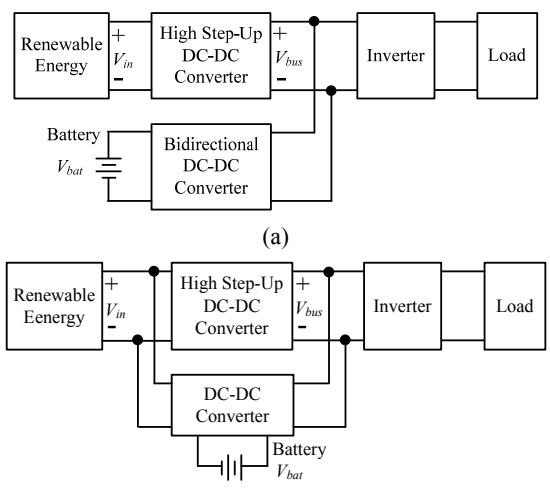

Fig. 1. Renewable energy and battery hybrid power supplies system. (a) Conventional type, (b) Three-port type.

Manuscript received Mar. 14, 2015; accepted May 18, 2015
Recommended for publication by Associate Editor Honnyong Cha.
†Corresponding Author: yanglungsheng@yahoo.com.tw
Tel: +886-6-5979566-5410, Far East University
*Department of Electrical Engineering, Far East University, Taiwan

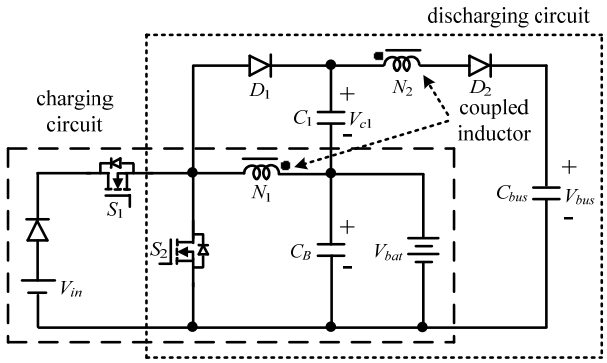

Fig. 2. Circuit configuration of proposed DC-DC converter.

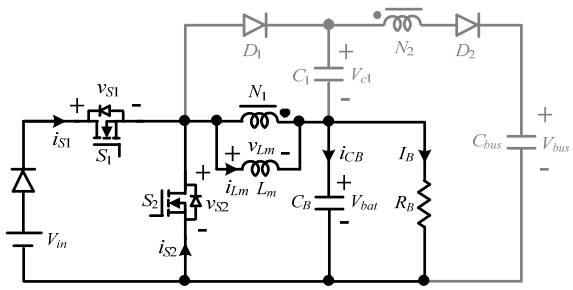

Fig. 3. Equivalent circuit of proposed converter at charging mode.

leakage-inductor energies of the primary and secondary windings can be recycled. Thus, only one power converter is utilized at the charging and discharging modes. The operating principles and steady-state analyses will be described in the following sections for the charging and discharging modes.

In order to analyze the steady-state characteristics of the proposed converter, some conditions are assumed: (1) Because the capacitors C_1, C_B, and C_{bus} are sufficiently large, the voltages across these capacitors can be treated as constant during each switching period. (2) The ON-state resistance of the switches, the forward voltage drop of the diodes, and the equivalent series resistances of the coupled inductor and capacitors are ignored.

II. CHARGING MODE

When the proposed converter is operated in the charging mode, the primary winding of the coupled inductor is used for a general inductor. The equivalent circuit of the proposed converter at the charging mode is shown in Fig. 3, where R_B is the equivalent load for the battery. The PWM technique is used to control switch S_1. Switch S_2 is used for the synchronous rectifier. Fig. 4 shows typical waveforms of the proposed converter with the continuous conduction mode (CCM) operation at the charging mode. The operating principles and steady-state analysis are described as follows:

1) Mode 1: During this time interval [t_0, t_1], switch S_1 is turned on and switch S_2 is turned off. The current flow path is shown in Fig. 5(a). The renewable-energy source V_{in} supplies its energy to for the coupled inductor L_m, capacitor C_B, and

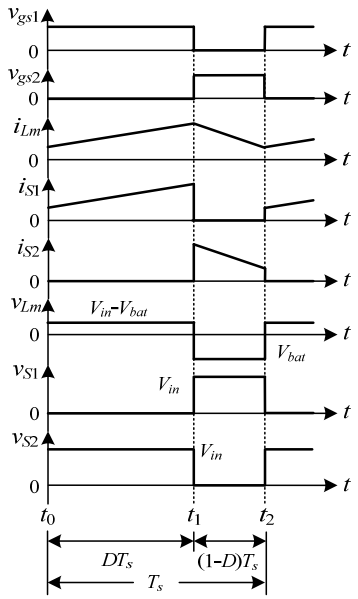

Fig. 4. Some typical waveforms of proposed converter with CCM operation at charging mode.

load R_B. Meantime, the coupled inductor L_m stores its energy. Thus, the current i_{Lm} is increased. The voltage across the coupled inductor L_m is given by:

$$v_{Lm(\mathrm{ON})} = V_{in} - V_{bat} \tag{1}$$

2) Mode 2: During this time interval [t_1, t_2], switch S_1 is turned off and switch S_2 is turned on. The current flow path is shown in Fig. 5(b). Meanwhile, switch S_2 is utilized for a synchronous rectifier. The energy stored in the coupled inductor L_m is released to the capacitor C_B and load R_B. The voltage across the coupled inductor L_m is derived as:

$$v_{Lm(\mathrm{OFF})} = -V_{bat} \tag{2}$$

By using the voltage-second balance principle on the coupled inductor L_m, the following equation is obtained:

$$v_{Lm(\mathrm{ON})} DT_s + v_{Lm(\mathrm{OFF})}(1-D)T_s = 0 \tag{3}$$

Substituting (1) and (2) into (3), the voltage gain in the charging mode is found to be:

$$M_{CCM} = \frac{V_{bat}}{V_{in}} = D \tag{4}$$

When the proposed converter is operated in the boundary conduction mode (BCM), typical waveforms are shown in Fig. 6. Thus, the peak value of the coupled-inductor current is written as:

$$I_{Lmp} = \frac{DT_s}{L_m}(V_{in} - V_{bat}) \tag{5}$$

By utilizing the ampere-second balance principle on the capacitor C_B, the following equation can be expressed as:

$$I_{CB} = \frac{\frac{1}{2} I_{Lmp} T_s - I_B T_s}{T_s} = 0 \tag{6}$$

From (6), the peak value of the coupled-inductor current can be rewritten as:

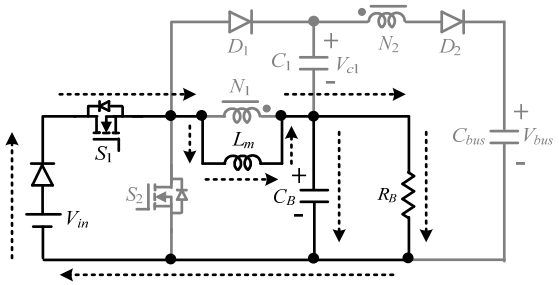

(a)

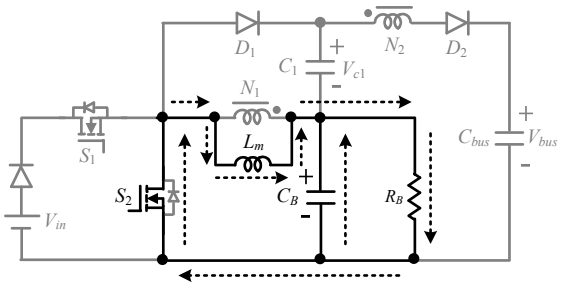

(b)

Fig. 5. Current flow path of proposed converter at charging mode. (a) Mode 1. (b) Mode 2.

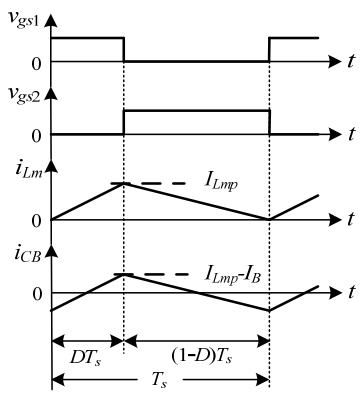

Fig. 6. Some waveforms of proposed converter with BCM operation at charging mode.

$$I_{Lmp} = 2I_B = \frac{2V_{bat}}{R_B} \tag{7}$$

Then, the normalized inductor time constant is defined as:

$$\tau_{Lm1} = \frac{L_m}{R_B T_s} \tag{8}$$

Substituting (4), (5), and (8) into (7), the boundary normalized inductor time constant is given by:

$$\tau_{Lm1,B} = \frac{1-D}{2} \tag{9}$$

If τ_{Lm1} is larger than $\tau_{Lm1,B}$, the proposed converter is operated in the CCM at the charging mode.

III. DISCHARGING MODE

The equivalent circuit of the proposed converter at the discharging mode is shown in Fig. 7, where R_L is the

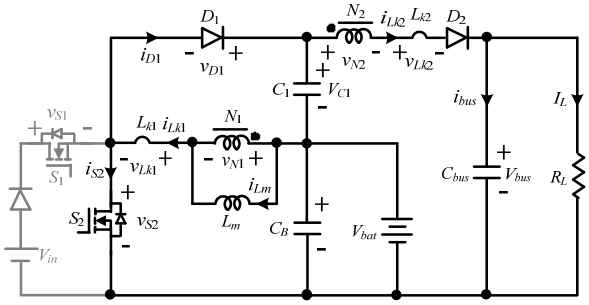

Fig. 7. Equivalent circuit of proposed converter at discharging mode.

equivalent load for the DC bus. The PWM technique is used to control switch S_2. Switch S_1 is turned off at the discharging mode. Fig. 8 shows typical waveforms of the proposed converter with the CCM operation at the discharging mode. The operating principles and steady-state analysis are described as follows:

1) Mode 1: During this time interval [t_0, t_1], switch S_2 is turned on. The current flow path is shown in Fig. 9(a). The energy of the battery is released to the magnetizing inductor L_m and primary leakage inductor L_{k1}. Thus, the currents i_{Lm} and i_{Lk1} are increased. The secondary leakage inductor L_{k2}, secondary winding N_2, capacitor C_1, and battery are in series to release their energies for the load R_L. The energy of the capacitor C_{bus} is also provided to the load R_L. Therefore, the current i_{Lk2} decreases. At $i_{Lk2} = 0$, the energy stored in the leakage inductor L_{k2} is completely recycled to the load R_L.

2) Mode 2: During this time interval [t_1, t_2], switch S_2 is still turned on. The current flow path is shown in Fig. 9(b). The energy of the battery is still released to the magnetizing inductor L_m and primary leakage inductor L_{k1}. The energy of the capacitor C_{bus} is provided to the load R_L.

3) Mode 3: During this time interval [t_2, t_3], switch S_2 is turned off. The current flow path is shown in Fig. 9(c). The energies stored in the magnetizing inductor L_m and primary leakage inductor L_{k1} are released the capacitor C_1. Thus, the currents i_{Lm} and i_{Lk1} are decreased. The secondary winding N_2, capacitor C_1, and battery are in series to release their energies for the leakage inductor L_{k2}, capacitor C_{bus}, and load R_L. Therefore, the current i_{Lk2} is increased. At $i_{Lk1} = 0$, the energy stored in the leakage inductor L_{k1} is completely recycled to the capacitor C_1.

4) Mode 4: During this time interval [t_3, t_4], switch S_2 is still turned off. The current flow path is shown in Fig. 9(d). The secondary leakage inductor L_{k2}, secondary winding N_2, capacitor C_1, and battery are in series to release their energies for the capacitor C_{bus} and load R_L. Therefore, the currents i_{Lm} and i_{Lk2} are decreased.

When switch S_2 is turned on, the following equation can be represented as:

$$v_{N1(ON)} + v_{Lk1(ON)} = V_{bat} \tag{10}$$

Thus:

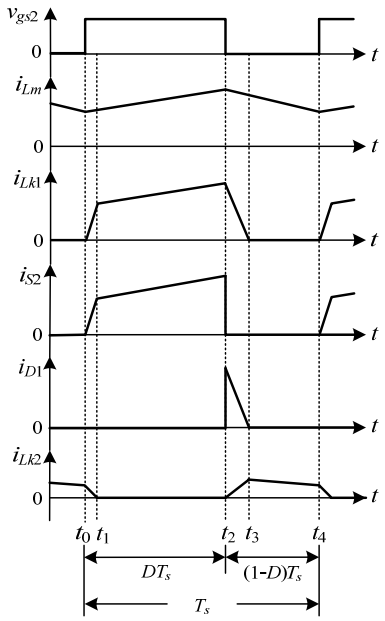

Fig. 8. Some typical waveforms of proposed converter with CCM operation at discharging mode.

$$v_{Lk1(\mathrm{ON})} = (1-k)V_{bat} \tag{11}$$

$$v_{N1(\mathrm{ON})} = kV_{bat} \tag{12}$$

$$v_{N2(\mathrm{ON})} = nv_{N1(\mathrm{ON})} = nkV_{bat} \tag{13}$$

where the turns ratio of the coupled inductor $n = N_2/N_1$, and the coupled coefficient $k = L_m/(L_m+L_{k1})$.

From the operating principle, it is known that the energy stored in the primary leakage inductor L_{k1} is recycled to the capacitor C_1. By using the ampere-second balance principle on the capacitor C_1, the released time duration of the primary leakage-inductor energy can be expressed as [20]:

$$t_r = t_3 - t_2 = \frac{2(1-D)}{1+n}T_s \tag{14}$$

By utilizing the voltage-second balance principle on the primary leakage inductor L_{k1} and magnetizing inductor L_m, the following equations can be obtained:

$$v_{Lk1(\mathrm{ON})}DT_s + v_{Lk1(tr)}t_r = 0 \tag{15}$$

$$v_{N1(\mathrm{ON})}DT_s + v_{N1(\mathrm{OFF})}(1-D)T_s = 0 \tag{16}$$

where $v_{Lk1(tr)}$ is the voltage across the primary leakage inductor L_{k1} during the time duration $[t_2, t_3]$ and the voltage $v_{N1(\mathrm{OFF})}$ across the magnetizing inductor L_m during the time duration $[t_2, t_4]$.

Substituting (11) and (14) into (15), yields:

$$v_{Lk1(tr)} = -\frac{(1-k)(1+n)D}{2(1-D)}V_{bat} \tag{17}$$

By substituting (12) into (16), it is possible to derive:

$$v_{N1(\mathrm{OFF})} = -\frac{kD}{1-D}V_{bat} \tag{18}$$

From Fig. 9(c), the following equation can be obtained:

$$V_{c1} + v_{Lk1(tr)} + v_{N1(\mathrm{OFF})} = 0 \tag{19}$$

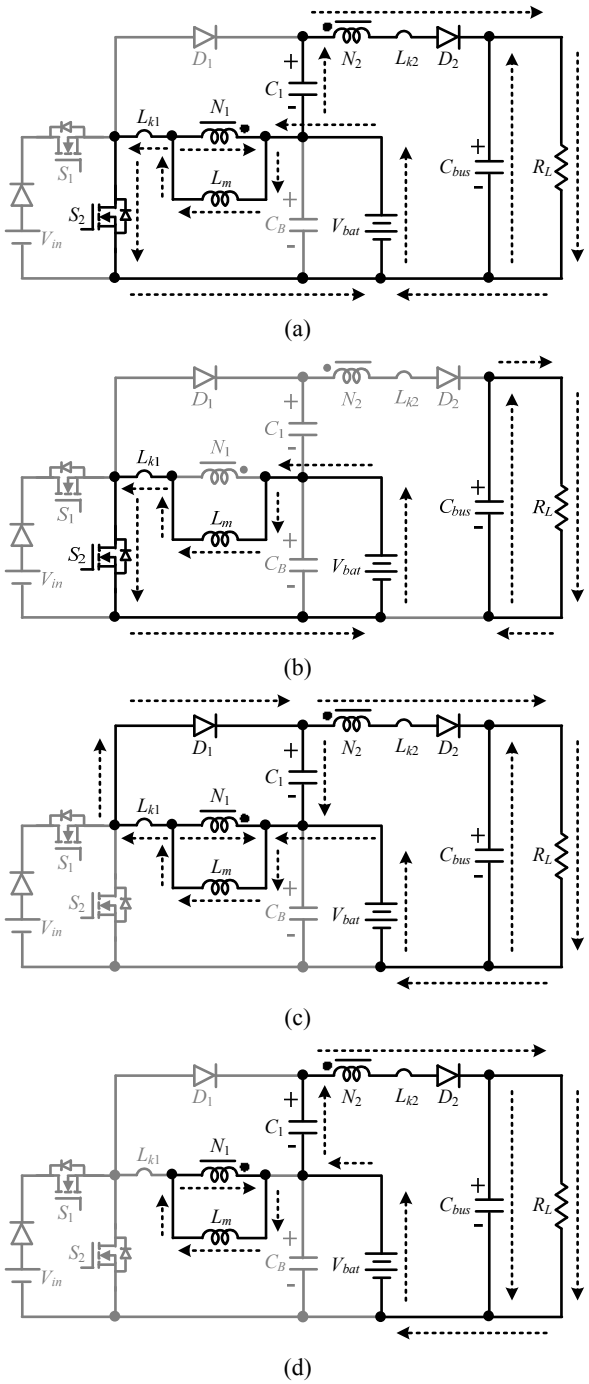

Fig. 9. Current flow path of proposed converter at discharging mode. (a) Mode1. (b) Mode 2. (c) Mode 3. (d) Mode 4.

Substituting (17) and (18) into (19), the voltage across the capacitor C_1 is written as follows:

$$V_{c1} = \frac{[n(1-k)+(1+k)]D}{2(1-D)}V_{bat} \tag{20}$$

During the switch S_2 OFF-period, the following voltage equation is found as:

$$V_{bat} + V_{c1} - V_{bus} = v_{N2(\mathrm{OFF})} + v_{Lk2(\mathrm{OFF})} = \frac{v_{N2(\mathrm{OFF})}}{k} \tag{21}$$

Therefore:

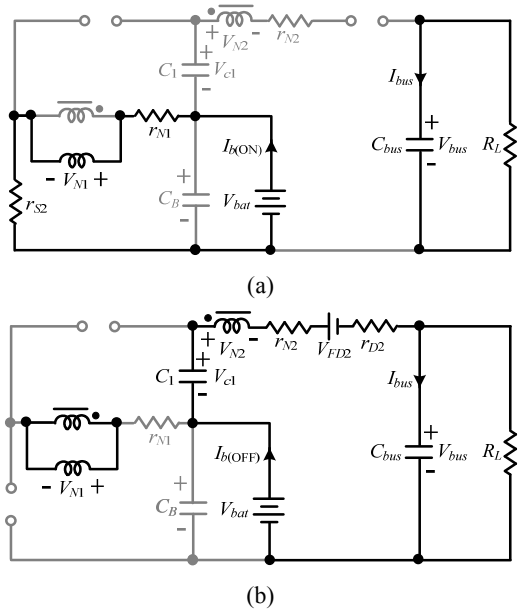

Fig. 10. Equivalent circuit including ESR of coupled inductor, ON-state forward voltage drop and resistance of diodes, and ON-state resistance of switch. (a) S_2 ON. (b) S_2 OFF.

$$v_{N2(\mathrm{OFF})} = k(V_{bat} + V_{c1} - V_{bus}) \tag{22}$$

Using the voltage-second balance principle on the secondary winding of the coupled inductor N_2, the equation can be represented as:

$$v_{N2(\mathrm{ON})} DT_s + v_{N2(\mathrm{OFF})}(1-D)T_s = 0 \tag{23}$$

Substituting (13), (20), and (22) into (23), the voltage gain can be found as follows:

$$M_{CCM} = \frac{V_{bus}}{V_{bat}} = \frac{2(1+nD)+(n-1)(1-k)D}{2(1-D)} \tag{24}$$

At k = 1, equation (24) is rewritten as:

$$M_{CCM} = \frac{V_{bus}}{V_{bat}} = \frac{1+nD}{1-D} \tag{25}$$

The voltage gain with parasitic components is analyzed as follows. In order to simplify the analysis, the leakage inductors of the coupled inductor are neglected. The equivalent circuit is shown in Fig. 10. r_{N1} and r_{N2} represent the equivalent series resistances (ESR) of the primary and secondary windings of the coupled inductor. V_{FD2} and r_{D2} are the ON-state forward voltage drop and resistance of D_2. r_{S2} denotes the ON-state resistance of S_2.

When switch S_2 is turned on, the equivalent circuit is shown in Fig. 10(a). The average values of i_{bus} and v_{N1} are written as:

$$I_{bus}^{I} = -\frac{V_{bus}}{R_L} \tag{26}$$

$$V_{N1}^{I} = V_{bat} - I_{b(\mathrm{ON})}(r_{N1} + r_{S2}) \tag{27}$$

When switch S_2 is turned off, the equivalent circuit is shown in Fig. 10(b). The average values of i_{bus} and v_{N1} are found as:

$$I_{bus}^{II} = I_{b(\mathrm{OFF})} - \frac{V_{bus}}{R_L} \tag{28}$$

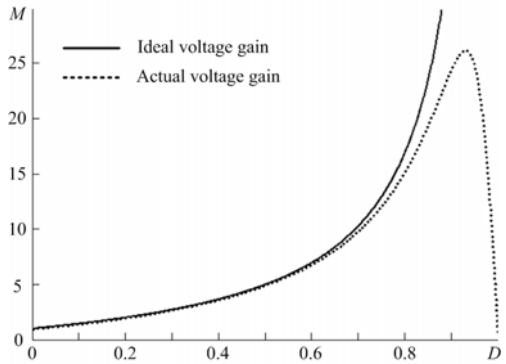

Fig. 11. Ideal and actual voltage gain in discharging mode.

$$V_{N1}^{II} = \frac{V_{bat} + V_{c1} - V_{FD2} - V_{bus} - I_{b(\mathrm{OFF})}(r_{N2} + r_{D2})}{n} \tag{29}$$

Since the leakage inductors of the coupled inductor are neglected, the coupling coefficient k is equal to 1. From (20), the voltage V_{c1} can be rewritten as:

$$V_{c1} = \frac{D}{1-D} V_{bat} \tag{30}$$

Substituting (30) into (29), yields:

$$V_{N1}^{II} = \frac{\frac{1}{1-D} V_{bat} - V_{FD2} - V_{bus} - I_{b(\mathrm{OFF})}(r_{N2} + r_{D2})}{n} \tag{31}$$

By using the ampere-second balance principle on C_{bus}, the following equations are obtained as:

$$\int_0^{DT_s} I_{bus}^{I} dt + \int_0^{(1-D)T_s} I_{bus}^{II} dt = 0 \tag{32}$$

Substituting (26) an (28) into (32), $I_{b(\mathrm{OFF})}$ is derived as:

$$I_{b(\mathrm{OFF})} = \frac{V_{bus}}{(1-D)R_L} \tag{33}$$

In addition, $I_{b(\mathrm{ON})}$ can be given as:

$$I_{b(\mathrm{ON})} = nI_{b(\mathrm{OFF})} = \frac{nV_{bus}}{(1-D)R_L} \tag{34}$$

Using the volt-second balance principle on L_m, yields:

$$\int_0^{DT_s} V_{N1}^{I} dt + \int_0^{(1-D)T_s} V_{N1}^{II} dt = 0 \tag{35}$$

Substituting (27), (31), (33), and (34) into (35), the actual voltage gain can be obtained as follows:

$$M = \frac{V_{bus}}{V_{bat}} = \frac{1+nD}{1-D} \times \frac{1 - \frac{1-D}{1+nD} \times \frac{V_{FD2}}{V_{bat}}}{1 + \frac{r_{N2} + r_{D2}}{(1-D)R_L} + \frac{n^2 D(r_{N1} + r_{S2})}{(1-D)^2 R_L}} \tag{36}$$

The curves of the ideal and actual voltage gain under n=3, r_{N1}=r_{N2}=100 mΩ, r_{D2}=50 mΩ, r_{S2}=50 mΩ, V_{FD2}=1.25 V, V_{bat}=24 V, and R_L=200 Ω are plotted in Fig. 11. It can be seen that the proposed converter in the discharging mode can achieve a high step-up voltage gain.

When the proposed converter is operating in the BCM, typical waveforms are shown in Fig. 12. Thus, the peak value of the magnetizing-inductor current is given as:

$$I_{Lmp} = \frac{kDT_s}{L_m} V_{bat} \tag{37}$$

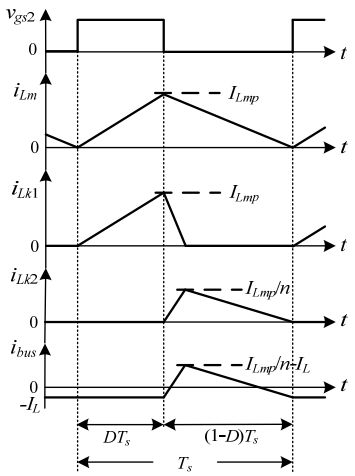

Fig. 12. Some waveforms of proposed converter with BCM operation at discharging mode.

Applying the ampere-second balance principle on the capacitor C_{bus}, the following equation is found:

$$I_{bus} = \frac{\frac{I_{Lmp}}{2n}(1-D)T_s - I_L T_s}{T_s} = 0 \tag{38}$$

From the above equation, the peak value of the magnetizing-inductor current is rewritten as:

$$I_{Lmp} = \frac{2n}{1-D} I_L = \frac{2nV_{bus}}{(1-D)R_L} \tag{39}$$

Then, the normalized inductor time constant is defined as:

$$\tau_{Lm2} = \frac{L_m}{R_L T_s} \tag{40}$$

Substituting (24), (37), (40) into (39), the boundary inductor time constant is obtained as follows:

$$\tau_{Lm2,B} = \frac{kD(1-D)^2}{n[2(1+nD)+(n-1)(1-k)D]} \tag{41}$$

At $k = 1$, τ_{Lm2} can be rewritten as:

$$\tau_{Lm2,B} = \frac{D(1-D)^2}{2n(1+nD)} \tag{42}$$

If τ_{Lm2} is larger than $\tau_{Lm2,B}$, the proposed converter in the discharging mode is operated in the CCM.

IV. Experimental Results

In order to verify the feasibility of the proposed converter, a prototype circuit is built for a fuel-cell and battery hybrid power supply system. The electric specifications and circuit components are selected as the input voltage V_{in} = 28~36.5 V, output power P_o = 200~20 W, battery voltage V_{bat} = 24 V, DC-bus voltage V_{bus} = 200 V, switching frequency f_s = 50 kHz, coupled inductor L_m = 72 μH and n = 3, capacitors $C_B = C_1 = C_{bus}$ = 220 μF, switches S_1 (IXFH80N085) and S_2 (IXTQ96N20P), and diodes D_1 (DSSK60-02AR) and D_2 (DSEP30-06A).

Fig. 13 shows the experimental results at the charging mode. The electrical specifications are V_{in} = 28 V, V_{bat} = 24 V, and full load P_o = 200 W. From Figs. 13(a) and 13(c), it can be seen that the current waveforms, i_{S1} and i_{Lm}, are same during the S_1 ON-period. As can be seen from Figs. 13(b) and 13(c), the current waveforms, i_{S2} and i_{Lm}, are the same during the S_1 OFF-period. Fig. 13(c) shows that the proposed converter is operated in the CCM. The measured efficiency at the charging mode is shown in Fig. 15. The measured efficiency is around 95.2%~97.5% under V_{in} = 28~36.5 V and P_o = 200~20 W. Fig. 14 shows the experimental results at the discharging mode. The electrical specifications are V_{bat} = 24 V, V_{bus} = 200 V, and full load P_o = 200 W. The waveforms, v_{gs2}, v_{S2}, and i_{S2}, are shown in Fig. 14(a). It can be seen from the waveform i_{S2} that the proposed converter is operated in the CCM. From the waveform v_{S2}, the voltage across S_2 is clamped at approximately 70 V during the S_2 OFF-period. Therefore, a low rated voltage MOSFET can be adopted to reduce the conduction loss. As shown in Fig. 14(b), the voltage across D_1 is clamped at approximately 70 V during the S_2 OFF-period. The waveforms, i_{D1} and i_{Lk1}, are shown in

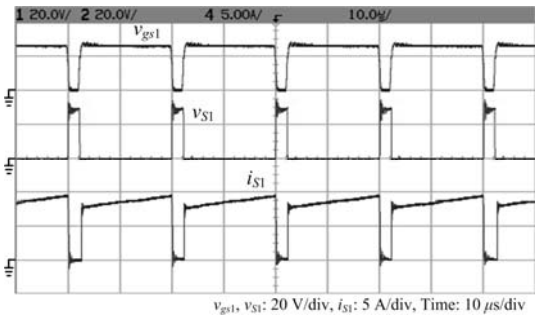

(a)

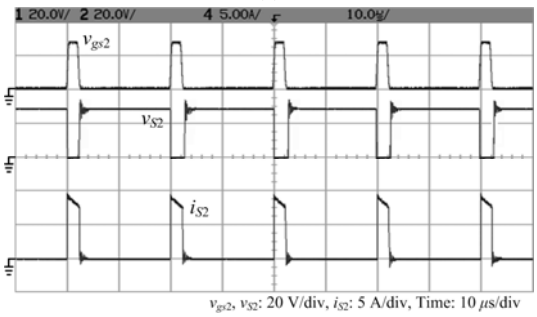

(b)

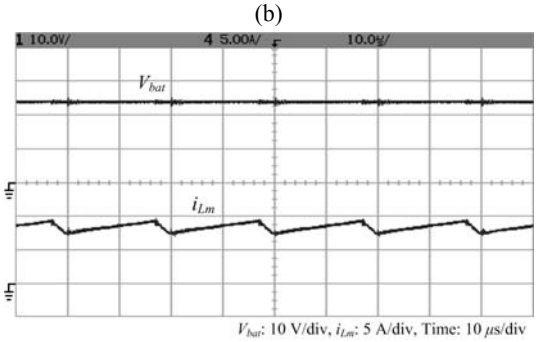

(c)

Fig. 13. Experimental waveforms of proposed converter at charging mode. (a) v_{gs1}, v_{S1}, i_{S1}, (b) v_{gs2}, v_{S2}, i_{S2}, (c) V_{bat}, i_{Lm}.

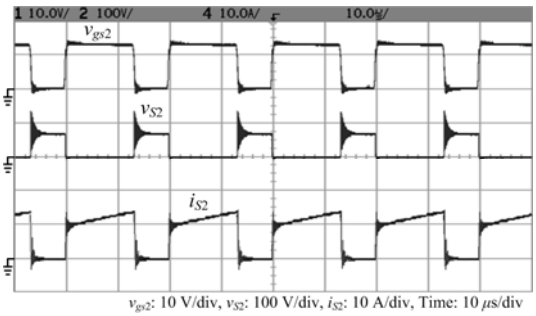

(a)

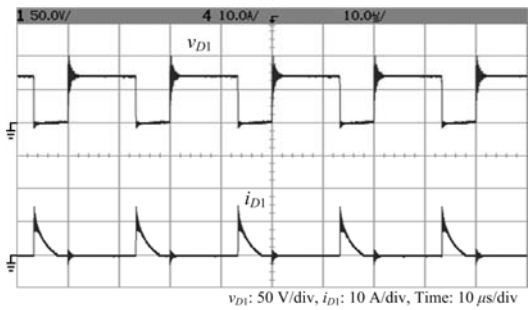

(b)

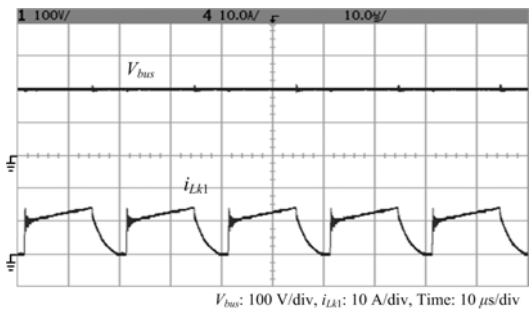

(c)

Fig. 14. Experimental waveforms of proposed converter at discharging mode. (a) v_{gs2}, v_{S2}, i_{S2}, (b) v_{D1}, i_{D1}, (c) V_{bus}, i_{Lk1}.

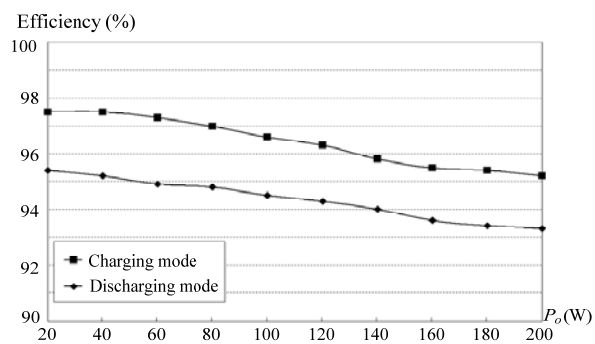

Fig. 15. Measured efficiency of proposed converter.

Figs. 14(b) and 14(c). It can be seen that they consist with the operating principle. The measured efficiency at the discharging mode is shown in Fig. 15. The measured efficiency is around 93.3%~95.4%.

V. CONCLUSIONS

In the conventional hybrid power supplied system, two power converters are used for the battery charging or discharging modes. The conventional system results in energy waste. A new DC-DC converter for renewable energy and battery hybrid power supplied systems is investigated in this paper. At the charging mode, a renewable energy source can provide its energy to charge the battery via the proposed converter. At the discharging mode, the battery can release its energy to the DC bus via the proposed converter. Thus, only one power converter is utilized at the charging or discharging modes. The proposed converter can increase the conversion efficiency. The measured efficiency is around 95.2%~97.5% at the charging mode and it is around 93.3%~95.4% at the discharging mode.

REFERENCES

[1] J. T. Bialasiewicz, "Renewable energy systems with photovoltaic power generators: operation and modeling," *IEEE Trans. Ind. Electron.*, Vol. 55, No. 7, pp. 2752-2758, Jul. 2008.

[2] J. M. Carrasco, L. G. Franquelo, J. T. Bialasiewicz, E. Galvan, R. C. P. Guisado, M. A. M. Prats, J. I. Leon, and N. M. Alfonso, "Power-electronic systems for the grid integration of renewable energy sources: a survey," *IEEE Trans. Ind. Electron.*, Vol. 53, No. 4, pp. 1002-1016, Aug. 2006.

[3] S. K. Kwon and K. F. A. Sayed, "Boost-Half bridge single power stage PWM DC-DC converter for PEM-fuel cell stacks," *Journal of Power Electronics*, Vol. 8, No. 3, pp. 239-247, Jul. 2008.

[4] F. Nejabatkhah, S. Danyali, S. H. Hosseini, M. Sabahi, and S. M. Niapour, "Modeling and control of a new three-input DC-DC boost converter for hybrid PV/FC/battery power system," *IEEE Trans. on Power Electron*., Vol. 27, No. 5, pp. 2309-2324, May 2012.

[5] T. Ahmedy, K. Nishida, and M. Nakaoka, "Wind power grid integration of an IPMSG using a diode rectifier and a simple MPPT control for grid-side inverters," *Journal of Power Electronics*, Vol. 10, No. 5, pp. 548-554, Sep. 2010.

[6] Y. L. Juan, "An integrated-controlled AC/DC interface for microscale wind power generation systems," *IEEE Trans. Power Electron*., Vol. 26, No. 5, pp. 1377-1384, May 2011.

[7] C. Xia, Q. Geng, X. Gu, T. Shi, and Z. Song, "Input-output feedback linearization and speed control of a surface permanent-magnet synchronous wind generator with the boost-chopper converter," *IEEE Trans. Ind. Electron.*, Vol. 59, No. 9, pp. 3489-3500, Sep. 2012.

[8] Y. M. Chen, A. Q. Huang, and X. Yu, "A high step-up three-port DC-DC converter for stand-alone PV/battery power systems," *IEEE Trans. Power Electron*., Vol. 28, No. 11, pp. 5049-5062, Nov. 2013.

[9] J. H. Lee, T. J. Liang, and J. F. Chen, "Isolated coupled inductor integrated DC-DC converter with non-dissipative snubber for solar energy applications," *IEEE Trans. Ind. Electron.*, Vol. 61, No. 7, pp. 3337-3348, Jul. 2014.

[10] H. M. Ryu, "Highly efficient AC-DC converter for small wind power generators," *Journal of Power Electronics*, Vol. 11, No. 2, pp. 188-193, Mar. 2011.

[11] Z. Liao and X. Ruan, "A novel power management control strategy for stand-alone photovoltaic power system," *IEEE International Power Electronics and Motion Control Conference*, pp. 445-449, 2009.

[12] S. J. Jang, T. W. Lee, W. C. Lee, and C. Y. Won, "Bi-directional DC-DC converter for fuel cell generation system," *IEEE Power Electronics Specialists Conference*, pp. 4722-4728, 2004.
[13] K. Jin, X. Ruan, M. Yang, and M. Xu, "A hybrid fuel cell power system," *IEEE Trans. Ind. Electron.*, Vol. 56, No. 4, pp. 1212-1222, Apr. 2009.
[14] D. K. Choi, B. K. Lee, S. W. Choi, C. Y. Won, and D. W. Yoo, "A novel power conversion circuit for cost-effective battery-fuel cell hybrid systems," *Journal of Power Sources*, Vol. 152, pp. 245-255, Dec. 2005.
[15] W. S. Liu, J. F. Chen, T. J. Liang, and R. L. Lin, "Multicascoded sources for a high-efficiency fuel-cell hybrid power system in high-voltage application," *IEEE Trans. Power Electron.*, Vol. 26, No. 3, pp. 931-942, Mar. 2011.
[16] W. Li, H. Wu, H. Yu, and X. He, "Isolated winding-coupled bidirectional ZVS converter with PWM plus phase-shift (PPS) control strategy," *IEEE Trans. Power Electron.*, Vol. 26, No. 12, pp. 3560-3570, Dec. 2011.
[17] A. S. Samosir and A. H. M. Yatim, "Implementation of dynamic evolution control of bidirectional DC-DC converter for interfacing ultracapacitor energy storage to fuel-cell system," *IEEE Trans. Ind. Electron.*, Vol. 57, No. 10, pp. 3468-3473, Oct. 2010.
[18] C. Sreekumar and V. Agarwal, "Hybrid control approach for the output voltage regulation in buck type DC-DC converter," *IET Electr. Power Appl.*, Vol. 1, No. 6, pp. 897-906, Nov. 2007.
[19] E. C. D. Santos, "Dual-output DC-DC buck converters with bidirectional and unidirectional characteristics," *IET Power Electron*., Vol. 6, No. 5, pp. 999-1009, May 2013.
[20] Q. Zhao and F. C. Lee, "High-efficiency, high step-up DC-DC converters," *IEEE Trans. Power Electron.*, Vol. 18, No.1, pp. 65-73, Jan. 2003.

Lung-Sheng Yang was born in Taiwan, ROC, in 1967. He received his B.S. degree in Electrical Engineering from the National Taiwan Institute of Technology, Taipei, Taiwan, in 1990; his M.S. degree in Electrical Engineering from National Tsing Hua University, Hsinchu, Taiwan, in 1992; and his Ph.D. degree in Electrical Engineering from National Cheng Kung University, Tainan, Taiwan, in 2007. He is presently working as an Assistant Professor in the Department of Electrical Engineering, Far East University, Tainan, Taiwan. His current research interests include power factor correction, dc-dc converters, renewable energy conversion, and electronic ballasts.

Chia-Ching Lin was born in Taiwan, ROC, in 1959. He received his B.S. degree from the Department of Electrical Engineering, Far East University, Tainan, Taiwan, in 1980; and his M.S. degree in Electrical Engineering from National Cheng Kung University, Tainan, Taiwan, in 2006. He is presently working as an Assistant Professor in the Department of Electrical Engineering, Far East University. His current research interests include power factor correction and dc-dc converters.